Impact of Equatorial Wind Change on the Meridional Heat Transport in the Atlantic

Sanjana Satish [1,2], Kaila Uyeda [2], C. Spencer Jones [2]

1. Indian Institute of Science Education and Research, Mohali

2. Texas A&M

*

ABSTRACT

Ocean heat transport in the Atlantic basin is northwards at all latitudes, and is largest between the equator and 42°N. This heat transport impacts multiple aspects of the Earth's climate, setting tropical precipitation, surface temperatures and Arctic sea ice concentration. In this paper, we attempt to understand the role of the equatorial winds in setting the meridional heat transport in the Atlantic using an idealized single basin model with a re-entrant channel in the southern boundary. Increasing the westward wind stress at the equator increases the volume transport of the subtropical cells. Although the wind stress changes are symmetric about the equator, we find that the heat transport in the Northern Hemisphere changes more than the heat transport in the Southern Hemisphere. We find that heat transport changes are mediated by the western boundary currents, which are warmer when the winds are stronger at the equator. This heat continues poleward until it reaches the poleward boundary of the subtropical gyre (STG), after which waters cool down due to exposure to colder subpolar atmospheric temperatures. A further series of experiments run with a 20% decrease in AMOC shows that the AMOC has very little impact on the fate of heat that enters the ocean in the equatorial Atlantic.

Significance statement. Optional significance statement goes here.

1. Introduction

The Atlantic Meridional Overturning Circulation (AMOC) is a large-scale system of ocean currents that plays a crucial role in Earth's climate by redistributing heat, salt, and nutrients. It consists of a northward-flowing upper limb, where warm, salty waters are transported to the North Atlantic, and a deep colder return flow, where dense waters formed in high-latitude polar sites sink and travel southward as the North Atlantic Deep Water (NADW) (see Broecker (1992), Richardson (2008)). The Atlantic Meridional Overturning Circulation causes the total ocean heat transport in the Atlantic to be northward at all latitudes (see (Trenberth and Caron 2001; Bryan 1962; Hastenrath 1982; Buckley and Marshall 2016; Kelly et al. 2014)). This feature of the heat transport in the Atlantic is unique among all ocean basins and has been recognized for its role in modulating the climate in the Europe (Palter 2015; Moffa-Sánchez and Hall 2017) and the Americas (Srokosz et al. 2012; Buckley and Marshall 2016; Lynch-Stieglitz 2017). Variations in the northward Atlantic heat transport are thought to be a key driver of Atlantic Multidecadal Variability (Oldenburg et al. 2021), which affects variability in multiple parts of the climate system (Zhang et al. 2019), including precipitation patterns (Folland et al. 1986; Martin and Thorncroft 2014).

While meridional Atlantic Ocean heat transport is northward at all latitudes, its magnitude varies significantly. The Atlantic Subtropical Cells (STCs) are shallow wind driven circulation patterns that connect the subtropics subduction areas to the tropical upwelling regions. The STCs transport water poleward at the surface and equatorward at depths of about 100-200m. (Tuchen et al. 2019). Heat transport by the subtropical cells has not been studied very much, (Klinger and Marotzke 2000) develops a theory to relate the heat transport to the winds over the subtropical cell. The theory directly correlates the heat transport to the Ekman transport, which they claim is bound within the subtropical cell.

Past the subtropical cells, the subtropical gyres extend to regions with negative wind stress curl. STGs each have a strong and narrow western boundary current that flows polewards, with a broader and slower return flow that is equatorwards in the rest of the basin Vallis (2017). Since each subtropical cell extends from the equator to the zero wind stress line, there is overlap between the subtropical gyres and the subtropical cells, and water parcels are exchanged between these structures (Rousselet and Cessi 2022). This study highlights how this exchange between the subtropical cell and the subtropical gyre impacts heat transport.

Studies in the past have attempted to separate the heat transport by the overturning circulation and by the gyres (Bryan 1962; Hall and Bryden 1982; McDonagh et al. 2010; Ferrari and Ferreira 2011; Piecuch et al. 2017; Bhagtani et al. 2024). While it is understood that the heat is transported northwards, these studies have shown that it is not straightforward to attribute this northward heat transport directly to either wind driven circulation or the buoyancy driven circulation, because winds affect the AMOC strength (Yang 2015; Cessi 2018), and buoyancy forcing affects the gyre profile (Bhagtani et al. 2023). In addition, both circulations interact, and some methods attribute a large fraction of the heat transport to the “mixed” circulation, which only occurs when both the AMOC and the gyres are present (Ferrari and Ferreira 2011; Bhagtani et al. 2024). Jones et al. (2024) compared several methods that separated the heat transport into gyre and overturning components and found that the results of these methods disagree: one possible explanation is that the mixed circulation dominates heat transport and separation into a contribution by the gyres and by the AMOC is not possible.

In this study, we do not aim to separate the contribution of the gyres and AMOC, instead we aim to characterize the relationship between winds at the equator, the overturning circulation and the meridional heat transport by running a series of model experiments with different equatorial winds in an idealized single basin Atlantic-like model. We find that the northward heat transport in the Northern Hemisphere increases with an increase in equatorial westward winds, and these heat transport differences extend to about 42°N. In the Southern Hemisphere, we see the heat transport differences, are of a lower magnitude than the North, and extend to about 30°S. We analyze the water pathways responsible for the transport of heat, and find that the observed heat transport differences are a result of the warmer waters primarily traveling through the western boundary currents of the subtropical gyres.

In our initial experiments, the wind stress over the Southern Ocean is higher than the wind stress over equivalent latitudes in the Northern Hemisphere, consistent with observations. Our initial experiments exhibit zonal asymmetries in heat transport, and we want to understand whether these asymmetries are caused by the asymmetric wind stress. Hence later in this paper we discuss further experiments with fully symmetric winds. The winds in this second set of experiments have a weaker wind stress over the Southern Ocean, which causes a weaker AMOC transport.

We first discuss our model set up and other relevant details of our run in Section 2. We discuss the heat transport and overturning from these simulations in Section 3. We then discuss the water pathways that may be responsible for the conduit of heat in both the hemispheres in Section 4. In Section 5 we discuss the set of experiments with reduced Southern Ocean winds. We conclude our results and discuss the summary in Section 6.

2. Data and Methods

The numerical model used is the Modular Ocean Model version 6 (MOM6) which uses a horizontal C-grid stencil and a vertical Lagrangian mapping. The ocean bathymetry is based on the NeverWorld2 model developed by Marques et al. (2022), but unlike the Neverworld2 configuration, which is adiabatic, our model has thermodynamics and convection. The domain is a spherical sector spanning 140° in latitude and 80° in longitude, enclosed by a solid coast at 70°N and 70°S; and also at 0°E and 80°E, except for a re-entrant channel at the southern edge of the basin centered at 50°S, as shown in Fig. 1. The model has a 1°×1° resolution, with 32 uneven depth layers - decreasing in resolution with increase in depth. The unevenly spaced layers range from a minimum spacing of 13m at the top to a maximum spacing of 309m at the bottom. A triangular ridge of height 2000m runs through the length of the basin, centered at 40°E with base spanning from 10°E to 70°E as shown in Fig. 1 (a). This ridge is an idealization of the Mid-Atlantic Ridge and Scotia Arc that work oppose momentum via drag across the Drake Passage.

The model is run with a linear equation of state described by

$$\rho = \rho_0 + \alpha_T T \tag{1}$$

where, ρ refers to the density of water, $\rho_0 = 1000 kg/m^3, \alpha_T = \frac{\partial\rho}{\partial T} = -0.2 kg/m^{3\circ}C$ The density is independent of salinity, i.e., the model is run with a constant salinity of 35ppm.

The surface temperature is relaxed towards a temperature profile that is shown in Fig. 1 (b), at a rate of $10 m/day$. Momentum dissipation is through Laplacian viscosity with horizontal and vertical viscosity coefficients $\nu_h = 2\times10^5 m^2/s$ and $\nu_v = 5\times10^{-6} m^2/s$ respectively. Because of the coarse resolution in the model, we use the parametrization of advective form from Gent and Mcwilliams (1990). This parameterization uses mixing coefficient $\kappa_{GM} = 500 m^2/s$. Because the salinity does not vary, there are no gradients of temperature along isopycnals and we do not parametrize the diffusive effects of eddies.

Our model is run with purely zonal wind stress ($\tau_y = 0$ everywhere), steady in time. The zonally averaged zonal wind forcings are shown in Fig. 2 (a). The expression for the zonal wind stress τ_x for seq0, our control case, is given by

$$\tau = \tau_{max}[-cos(3\pi\theta) + e^{-\theta^2/2\sigma_1^2} + e^{-(\theta+46.7)^2/2\sigma_2^2}] \tag{2}$$

where τ_{max} = 0.1Pa, σ_1=10°, and σ_2=8°. The rightmost exponential term is responsible for creating stronger eastward winds over the Southern Ocean than at equivalent latitudes in the Northern Hemisphere (see Fig. 2). In perturbation experiments (here called seq2, seq and seq4.6) the equatorial wind stress is changed by adding weighted Gaussian bumps centered around the equator, as seen in Fig. 2. Differences between the cases are localized close to the equator between 12.5°N and 12.5°S.

a. Residual Overturning Streamfunction

1) Depth Space

The overturning circulation is quantified using the zonally integrated residual overturning streamfunction

$$\psi(y,z,t) = \int_0^{L_x}\int_0^{H} v^{\dagger}(x,y,z,t)\,dz\,dx \tag{3}$$

where $v^{\dagger}$ is the resolved velocity plus the eddy velocity from the GM parametrization, H is the ocean depth and L_x is the width of the basin.

Winds close to the equator are westwards, and this drives a poleward Ekman transport in both hemispheres. The shaded contours in Fig. 3 show the residual overturning circulation in depth space in the between 25°S and 25°N. Our subtropical cells are contained within the latitudes of the zero wind stress line containing the equator, which is from 23 $^\circ S$ to 23 $^\circ N$. We choose to zoom in on these latitudes in Fig. 3 because of the negligible change in the streamfunction outside of these latitudes (see supplement).

To illustrate the theoretical volume transport due to wind-driven velocities in this region, we employ the vertical streamfunction due to wind stress formulated by Rousselet and Cessi (2022), where the streamfunction proportional to the wind stress forcing is given by

$$\phi(y,z) = -\frac{\tau_x(y,0)}{\rho f}\left(1+\frac{z}{H}\right) \tag{4}$$

where f is the Coriolis parameter, and H is the maximum depth, which we set as 400m in our calculations. This calculation gives us the theoretical wind driven circulation in the top 400m of the ocean as a function of latitude and depth, which are shown in the black contours in Fig. 3.

2) Density Space

The overturning circulation as a function of latitude and density is quantified using

$$\psi_\rho(y,\tilde{\rho},t) = \int_0^{L_x}\int_{z(\tilde{\rho})}^{z(\rho_s)} v^\dagger(x,y,z(\rho),t)\,dz\,dx\,, \tag{5}$$

where ρ_s is the density at the surface. The variable ψ_ρ is then the zonally integrated transport of water as a function of latitude and density, as shown in Fig. 4.

3. Results

We show the heat transport for each of the wind forcings in Fig. 2(b). Fig. 2 (c) shows the difference in heat transport between the simulations with westward equatorial winds (seq2, seq3, and seq4.6) and the control run (seq0). We see an increase in the northward heat transport with an increase in westwards winds at the equator. In the Northern Hemisphere we observe that the difference in the heat transport in the westward wind cases continues up to 42°N. We see that in the Southern Hemisphere, there is a decrease in the heat transported southwards with an increase in wind strength, and this difference is negligible polewards of 30°S. Hence, an equatorially symmetric change in wind stress between 12.5°S and 12.5°N leads to an equatorially asymmetric change in heat transport between 30°S and 42°N.

To better understand how the differences in heat transport arise, we next examine the overturning streamfunction calculated in depth space. We plot the ROC for seq0 in Fig. 3(a) and the difference from seq0 for the other 3 wind stresses cases in Fig. 3 (b), (c), (d). The transport of the subtropical cells increases with an increase in the winds, and these changes are roughly symmetric around the equator in all 3 cases. We see the difference primarily localized around the equator, confined to 25°S and 25°N, in the subtropical cell.

We plot the theoretical streamlines, as defined above in eq. (4) as contours overlapping the shaded ROC in Fig. 3. The theoretical Ekman transport is largest at the equator because f is zero there, and for the same reason, the differences between the theoretical transports from different winds are also largest at the equator (0.5°S and 0.5°SN where the grids are defines). But the maximum difference in the simulation appears to be centered around about 5°N and 5°S. This is likely caused by viscous effects, which are not included in the theoretical predictions.

Although the theoretical Ekman streamline contour differences only extend up to 12.5° in both hemispheres, as expected due to the wind change latitudes, the actual ROC differences extend beyond these latitudes and depths in all of the wind cases. The depth of the volumetric transport difference increases in both hemispheres with an increase in winds at the equator, meaning that colder waters from deeper depths are upwelled at the equator when the winds increase. This allows for ventilation of colder waters at the equator, resulting in a net heat uptake.

We observe that the volume transport of water in depth space cannot explain the transport of heat from the equator, because while the ROC differences appear to be symmetric around the equator, the heat transport differences are not. Furthermore, the heat transport differences occur farther northwards than the observed ROC differences do. The change in the volume transport of water in the subtropical cell cannot be responsible for the meridional heat transport of water, which extends further polewards in both hemispheres.

The overturning circulation is calculated as a function of density and latitude as described in Section 2. We plot the ROC in density space for seq0 in Fig. 4 (a) and the difference between the other wind stress cases and seq0 in Fig. 4(b), (c) and (d). We notice that the maximum difference is confined to the lower densities. We see a larger change in the volumetric transport in the Northern Hemisphere, in comparison to the South. An increase in wind corresponds to a larger volume transport of water in the density range of 1023 to 1026. The difference in ROC streamfunction in density space continues farther north than the differences in the ROC streamfunction in depth space, reaching 42°N. Density and temperature have a linear relationship in our model (eq. (1)), so any changes in the ROC in density space can be attributed to the changes in the temperature of water flow. Hence, the circulations that we see in density space are always associated with warmer water flowing in one direction and colder water flowing in the other direction.

Fig. 5 shows the barotropic streamfunction of the circulation showing the tropical, subtropical and subpolar gyres, and we note that the northern edge of the subtropical gyre in the Northern Hemisphere is at 42°N. The changes in the density space ROC (see Fig. 4) in the Northern Hemisphere extend to the poleward boundary of the subtropical gyre (blue lines) in all of the wind cases. The subtropical gyre in the Southern Hemisphere is bound by the ACC, and has a lower latitude extent in the western boundary of the basin. The latitude of changes in the density space ROC (see Fig. 4) in the Southern Hemisphere lie at a lower latitude of about 30°S. The asymmetry in the density ROC differences aligns well with the asymmetry of the heat transport differences in Fig. 2(c). We conclude that the increased heat transport till the subtropical gyre boundary is the result of the increased temperatures of water flowing northwards; and this change only gets stronger when we have stronger winds at the equator. In the next section, we will explore the pathway of this high-temperature water.

4. Water Pathways responsible for the Heat Transport

As discussed in Section 3, the increased heat transport from the equator to the is due to an increased volume of high-temperature water flowing till the STG edge. The volume of water that changes in the subtropical cell is recirculated in the tropics, and does not extend farther. To examine the water pathways of the higher temperature waters responsible for this, we plot the longitudinal cross-section of the isopycnals from the equator till 40°N and 30°S varying in 20° and 10° intervals in both hemispheres respectively, as seen in Fig. 6 and Fig. 7.

Fig. 6 and Fig. 7 show the cross-section of the isopycnals in both Hemispheres. Fig. 6(a) shows the isopycnals at the Equator. The isopycnals are more tilted when the winds are stronger. This difference is highest at the equator and the tropics – to which we have limited our wind changes. Analysis of the isopycnals as plotted in Fig. 6 suggests that the difference in the depths of isopycnals are most prominent in the western boundary of the basin. These differences in the WBCs continue till about 40°N. At a given depth, water at the WBC of a higher equatorial wind forcing will be warmer than that of a lower equatorial wind forcing. The temperature of the water at a given depth and latitude is warmer at the western boundary, if the winds at the equator are stronger, thus contributing to a higher magnitude of heat transport. The equator is a region of high upwelling of waters, which increases with an increase in winds, thus, enabling ventilation of larger volumes of water. The volumes of water flowing changes only as far as the subtropical cell, which might be due to an increased strength in the recirculation of waters in the tropics itself. But the waters that do continue traveling polewards beyond the tropics (via the western boundary currents), are warmer if the winds at the equator are higher.

At the poleward edge of the Northern Hemisphere subtropical gyre, the western boundary current separates from the boundary, and travels eastwards, instead of going farther north. This exposes warm waters to the cold atmospheric conditions of the subtropics, leading to a net heat flux from the ocean to the atmosphere at these latitudes, which may set the boundary of heat transport differences we notice in Fig. 2 (c). We also see this in Fig. 8 which shows the net surface heat flux of the ocean. The heat uptake is highest at the equator in the eastern parts of the basin where colder waters upwell. Highest loss of heat happens at the western boundary at the STG latitudes. This loss of heat also continues eastwards in the basin. Colder waters then downwell at these latitudes, from where they travel equatorwards, as seen in Fig. 6 via the eastern boundary of the basin. Waters then upwell at the equator from the east, completing the circuit.

We isolate and simplify the northward pathway of water from the equator in Fig. 15. Water upwells at the equator, warms, and flows north through the western boundary current till the northern edge of the STG, at which point they cool, downwell and travel equatorwards via the easternmost flow of the basin.

Fig. 2 shows that in the Southern Hemisphere, the difference in heat transport between seq0 and the experiment forcings only exist until about 30°S. Although the poleward boundary of the subtropical gyre extends farther south than this, the presence of the Antarctic Circumpolar Current (ACC) causes the subtropical gyre extent to separate from the western boundary at about 30°S. This can be seen in the barotropic streamfunctions plotted in Fig. 5. The subtropical gyre in the Southern Hemisphere extends only up to 30°S in the western boundary, but extends farther south in the east beyond 40°E. Since we have seen that the higher temperature waters flow through the western boundary circulation, the heat transported only extends as far south as the subtropical gyre's western boundary current.

5. Heat Transport with Symmetric Zonal Winds

Next, we run the equatorial winds with a weaker wind forcing over the Southern Ocean, making the wind profile symmetric around the equator throughout the length of the basin. This is done to understand if the observed asymmetry in the heat transport differences is a result of the equatorial asymmetry in the winds.

The wind profile and the heat transport for these new simulations are shown in Fig. 10. The most striking result is, despite an equatorially symmetric wind stress forcing, we still observe an asymmetry in the heat transported across the equator to both hemispheres. While the magnitude of heat being transported is higher in the Northern Hemisphere with an increased Southern Ocean winds, we see that the changes in the heat transport with in the eqx experiments (eqx-eq0) remain very similar to the changes we observe in the seqx experiments (Fig. 2(c) and Fig. 10(c)). Change in the state of the AMOC (and hence an increased volume transport) causes the heat transport to increase by the same amount for all of the corresponding equatorial winds (notice how the differences follow very similar values and trends at lower latitudes (Fig. 10)). The zonal heat transport difference, however, changes negligibly (see supplement).

We see the volume transport contours in density space at the equator for both the experiment runs in Fig. 11. We see that the maximum AMOC flow in eqx experiments is 20.6% lower than the peak transport flow in seqx. We also plot Fig. 13 which shows the difference between eq0 and eqx residual overturning circulation in the density space. We have seen in Section 4 that the difference in heat transport between seq0 and seqx is a result of the change in temperature of the waters flowing from the equator. We see that Fig. 13 also follows the same result – the differences in the heat transport in the eqx series extend till the poleward edge of STG in the Northern Hemisphere, and till the poleward edge at the western basin of the STG in the Southern Hemisphere (see Fig. 12 which shows that the gyre boundaries of the eqx experiments). This confirms that the pathways of water carrying heat over the basin remain largely similar in both the seqx and eqx experiments. Reduced Southern Ocean wind stress does not alter heat transport pathways.

The heat transport differences remain asymmetric, with larger difference in the Northern Hemisphere compared to the Southern Hemisphere for all of the wind cases. The shape and magnitude of the changes due to equatorial wind stress are not affected by the change in AMOC transport. Hence, the asymmetry in the heat transport does not appear to arise from the asymmetry in the zonal wind profile in Fig. 2 (a). The geometry of the basin, however, is retained in all the runs. The ocean basin in all the runs is asymmetric around the equator, due to the presence of the re-entrant channel in the Southern boundary. The presence of the Antarctic Circumpolar Current forces the boundary of the Southern subtropical gyre to be closer to the equator, thus the warm boundary currents have a lower latitude extent. This is the most likely the cause of the asymmetry in heat transport about the equator.

6. Concluding Remarks

One goal of this study was to understand the relationship between winds at the equator and the northward heat transport in the AMOC. We ran a series of increasingly westwards wind models at the equator, each run with symmetric and asymmetric high latitude winds. We compared it with a control run that was set at 0 Pa at the equator. In response to these changes in wind, the zonally-integrated circulation in depth space displayed significant differences within 25° of the equator. But we find that the effects of westward wind changes close to the equator on the heat transport extend to the poleward boundary of the subtropical gyre: about 42°N in the Northern Hemisphere and about 30°S in the Southern Hemisphere.

The equator is a site of high Ekman upwelling, and this upwelling increases with increasing winds, leading to more heat uptake. Previous theoretical work by Klinger and Marotzke (2000) predicted that the heat transport differences are contained purely within the subtropical cell. We find that this is not true for an Atlantic-like basin: the heat transport differences extend as far as the poleward edge of the subtropical gyre, and the change in the heat transported due to tropical winds is barely affected by changes to the buoyancy forcing and the AMOC.

As westward wind stress at the equator increases, the volume of water traveling poleward due to Ekman transport increases. At the equator, this strengthened divergence causes more cool water to upwell and warm at the surface. The temperatures of water in the western boundary increases with an increase in the wind. This warm water is eventually transported northwards in the western boundary. The volume of waters transported outside the subtropical cell do not change in response to the change in winds at the equator, but these waters are warmer when the winds stress is higher.

An increase in volume of warmer waters traveling along the western boundary of the subtropical gyre appears to be responsible for the transport of heat from the equator. At the poleward boundary of the subtropical gyre these warm waters sink and travel equatorwards at deeper depths. Fig. 15 shows a simplified version of the water pathways carrying warm waters to the Northern Hemisphere. The water pathways we infer are similar to Fig. 18 in Rousselet and Cessi (2022) which shows the particle trajectories in the Northern Hemisphere, and how they are connected between the tropical and subtropical gyres and the subtropical cell.

Despite zonally symmetric wind changes, the transport of heat is zonally asymmetric over the basin, and this asymmetrical nature is not influenced by the strength of winds over the equator. In the second set of experiments, we employ a symmetric wind forcing over the basin, which means that the only changes between the two hemispheres are in the geometry and the temperature forcing. The re-entrant channel in the Southern Hemisphere allows for an Antarctic Circumpolar Current, which could be responsible for the asymmetry in the heat transport. Due to the geometry, and consequently the presence of the ACC, the western boundary of the subtropical gyre in the SH lies at a lower latitude than the corresponding eastern parts of the gyre. Since warmer waters travel primarily through the western boundary currents, the warmer waters in the SH are bound by the ACC in the westernmost part of the basin, which extends less polewards than the WBCs in STG in the NH. The latitudes of separation of the gyre and the subtropical cell in our model's basin is different from the real geometry of the ocean. In the Northern Hemisphere, the subtropical gyre flows through the Gulf stream past Cape Hatteras at 35°N off the coast of North Carolina. The North Atlantic Current arising from the Gulf Stream from the Grand Banks of Newfoundland at $45^/circ$N, and extending into the Norwegian Sea off northwestern Europe marks the separation of the subtropical and the subpolar gyres. The poleward extent of the Souther STG lies around south Brazil at Río de la Plata, where the southward flowing Brazil Current is met with the Falkland Currents at the Brazil-Malvinas Confluence Zone. This zone occurs between 35° to 45°S. Our experiments run on the ideal geometry of the ocean basin are important in understanding the role of these locations of separations to the transport of heat in the AMOC.

Acknowledgments. CSJ would like to acknowledge funding support from NSF Award Number OCE-2219852.

Data availability statement. The code used to generate these plots can be found on this Github repository - `https://github.com/Sanjanaa-19/Equatorial_wind`

References

Bhagtani, D., A. M. Hogg, R. M. Holmes, and N. C. Constantinou, 2023: Surface heating steers planetary-scale ocean circulation. *Journal of Physical Oceanography*, **53 (10)**, 2375–2391.

Bhagtani, D., A. M. Hogg, R. M. Holmes, and N. C. Constantinou, 2024: Unraveling how winds and surface heat fluxes control the atlantic ocean's meridional heat transport. *arXiv preprint arXiv:2401.14230*.

Broecker, W. S., 1992: The great ocean conveyor. *Global warming: physics and facts*, **247**, 129–161.

Bryan, K., 1962: Measurements of meridional heat transport by ocean currents. *Journal of Geophysical Research*, **67 (9)**, 3403–3414.

Buckley, M. W., and J. Marshall, 2016: Observations, inferences, and mechanisms of the atlantic meridional overturning circulation: A review. *Reviews of Geophysics*, **54 (1)**, 5–63.

Cessi, P., 2018: The effect of northern hemisphere winds on the meridional overturning circulation and stratification. *Journal of Physical Oceanography*, **48 (10)**, 2495–2506.

Ferrari, R., and D. Ferreira, 2011: What processes drive the ocean heat transport? *Ocean Modelling*, **38 (3-4)**, 171–186.

Folland, C. K., T. N. Palmer, and D. E. Parker, 1986: Sahel rainfall and worldwide sea temperatures, 1901–85. *Nature*, **320 (6063)**, 602–607.

Gent, P. R., and J. C. Mcwilliams, 1990: Isopycnal mixing in ocean circulation models. *Journal of Physical Oceanography*, **20 (1)**, 150–155.

Hall, M. M., and H. L. Bryden, 1982: Direct estimates and mechanisms of ocean heat transport. *Deep Sea Research Part A. Oceanographic Research Papers*, **29 (3)**, 339–359.

Hastenrath, S., 1982: On meridional heat transports in the world ocean. *Journal of Physical Oceanography*, **12 (8)**, 922–927.

Jones, C. S., S. Jiang, and R. P. Abernathey, 2024: A comparison of diagnostics for amoc heat transport applied to the cesm large ensemble. *Journal of Advances in Modeling Earth Systems*, **16 (8)**, e2023MS003 978.

Kelly, K. A., L. Thompson, and J. Lyman, 2014: The coherence and impact of meridional heat transport anomalies in the atlantic ocean inferred from observations. *Journal of Climate*, **27 (4)**, 1469–1487.

Klinger, B. A., and J. Marotzke, 2000: Meridional heat transport by the subtropical cell. *Journal of physical oceanography*, **30 (4)**, 696–705.

Lynch-Stieglitz, J., 2017: The atlantic meridional overturning circulation and abrupt climate change. *Annual review of marine science*, **9 (1)**, 83–104.

Marques, G. M., and Coauthors, 2022: Neverworld2: An idealized model hierarchy to investigate ocean mesoscale eddies across resolutions. *Geoscientific Model Development*, **15 (17)**, 6567–6579.

Martin, E. R., and C. D. Thorncroft, 2014: The impact of the amo on the west african monsoon annual cycle. *Quarterly Journal of the Royal Meteorological Society*, **140 (678)**, 31–46.

McDonagh, E. L., P. McLeod, B. A. King, H. L. Bryden, and S. T. Valdés, 2010: Circulation, heat, and freshwater transport at 36 n in the atlantic. *Journal of Physical Oceanography*, **40 (12)**, 2661–2678.

Moffa-Sánchez, P., and I. R. Hall, 2017: North atlantic variability and its links to european climate over the last 3000 years. *Nature Communications*, **8 (1)**, 1726.

Oldenburg, D., R. C. Wills, K. C. Armour, L. Thompson, and L. C. Jackson, 2021: Mechanisms of low-frequency variability in north atlantic ocean heat transport and amoc. *Journal of Climate*, **34 (12)**, 4733–4755.

Palter, J. B., 2015: The role of the gulf stream in european climate. *Annual review of marine science*, **7 (1)**, 113–137.

Piecuch, C. G., R. M. Ponte, C. M. Little, M. W. Buckley, and I. Fukumori, 2017: Mechanisms underlying recent decadal changes in subpolar n orth a tlantic o cean heat content. *Journal of Geophysical Research: Oceans*, **122 (9)**, 7181–7197.

Richardson, P. L., 2008: On the history of meridional overturning circulation schematic diagrams. *Progress in Oceanography*, **76 (4)**, 466–486.

Rousselet, L., and P. Cessi, 2022: Diabatic transformations along the global routes of the middepth meridional overturning circulation. *Journal of Physical Oceanography*, **52 (12)**, 3159–3177.

Srokosz, M., M. Baringer, H. Bryden, S. Cunningham, T. Delworth, S. Lozier, J. Marotzke, and R. Sutton, 2012: Past, present, and future changes in the atlantic meridional overturning circulation. *Bulletin of the American Meteorological Society*, **93 (11)**, 1663–1676.

Trenberth, K. E., and J. M. Caron, 2001: Estimates of meridional atmosphere and ocean heat transports. *Journal of Climate*, **14 (16)**, 3433–3443.

Tuchen, F. P., J. F. Lübbecke, S. Schmidtko, R. Hummels, and C. W. Böning, 2019: The atlantic subtropical cells inferred from observations. *Journal of Geophysical Research: Oceans*, **124 (11)**, 7591–7605.

Vallis, G. K., 2017: *Atmospheric and oceanic fluid dynamics*. Cambridge University Press.

Yang, J., 2015: Local and remote wind stress forcing of the seasonal variability of the atlantic meridional overturning circulation (amoc) transport at 26.5 n. *Journal of Geophysical Research: Oceans*, **120 (4)**, 2488–2503.

Zhang, R., R. Sutton, G. Danabasoglu, Y.-O. Kwon, R. Marsh, S. G. Yeager, D. E. Amrhein, and C. M. Little, 2019: A review of the role of the atlantic meridional overturning circulation in atlantic multidecadal variability and associated climate impacts. *Reviews of Geophysics*, **57 (2)**, 316–375.

LIST OF FIGURES

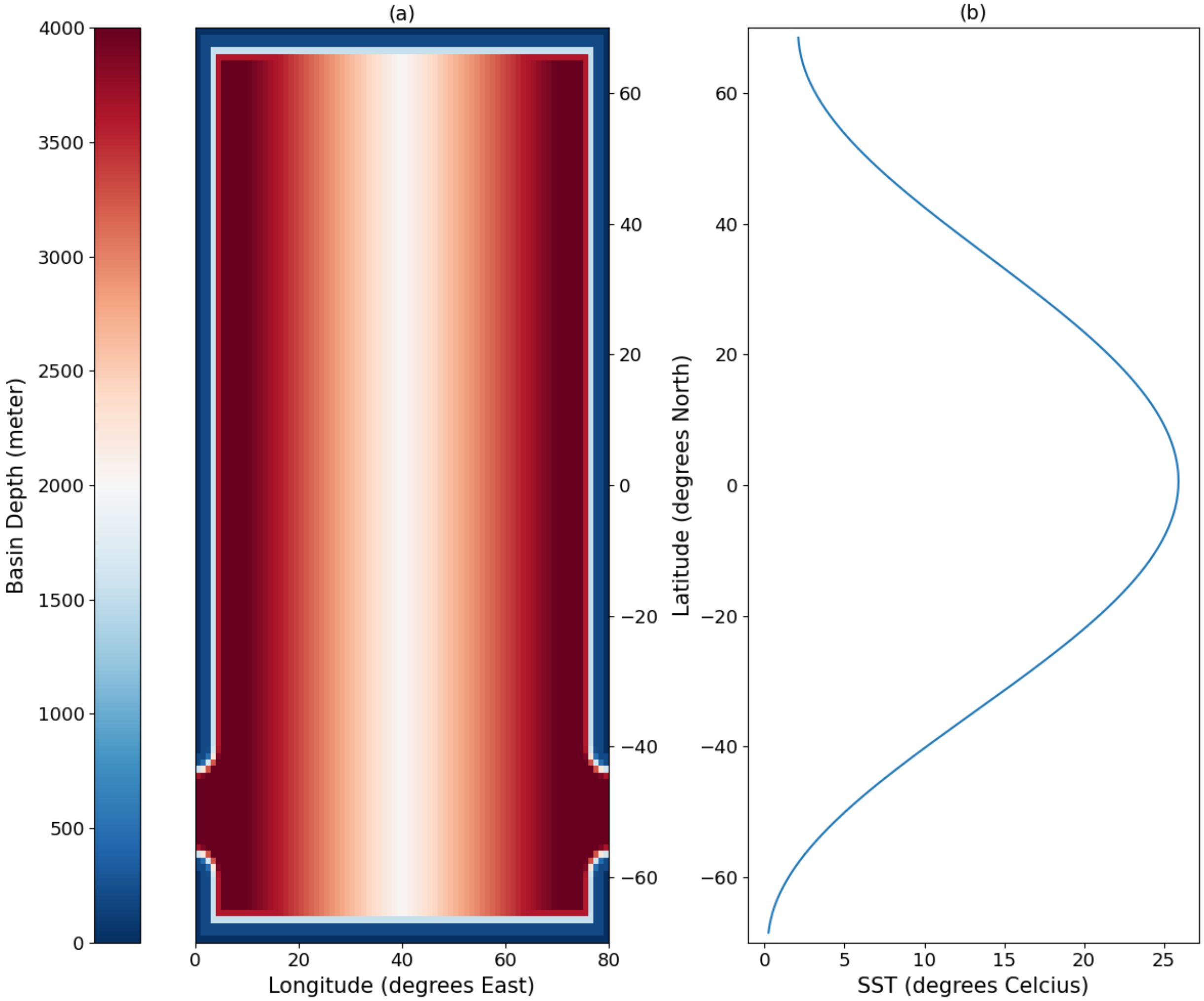

FIG. 1. (a) 2D Bathymetry - Depth in meters. The basin has a re-entrant channel in the Southern Ocean, centered around 50°S. A triangular ridge running through the length of the basin is an idealization of the Mid-Atlantic Ridge; (b) Latitude profile of zonally averaged SST forcing. The sea surface temperature is relaxed towards this profile at a rate of 10 m/day

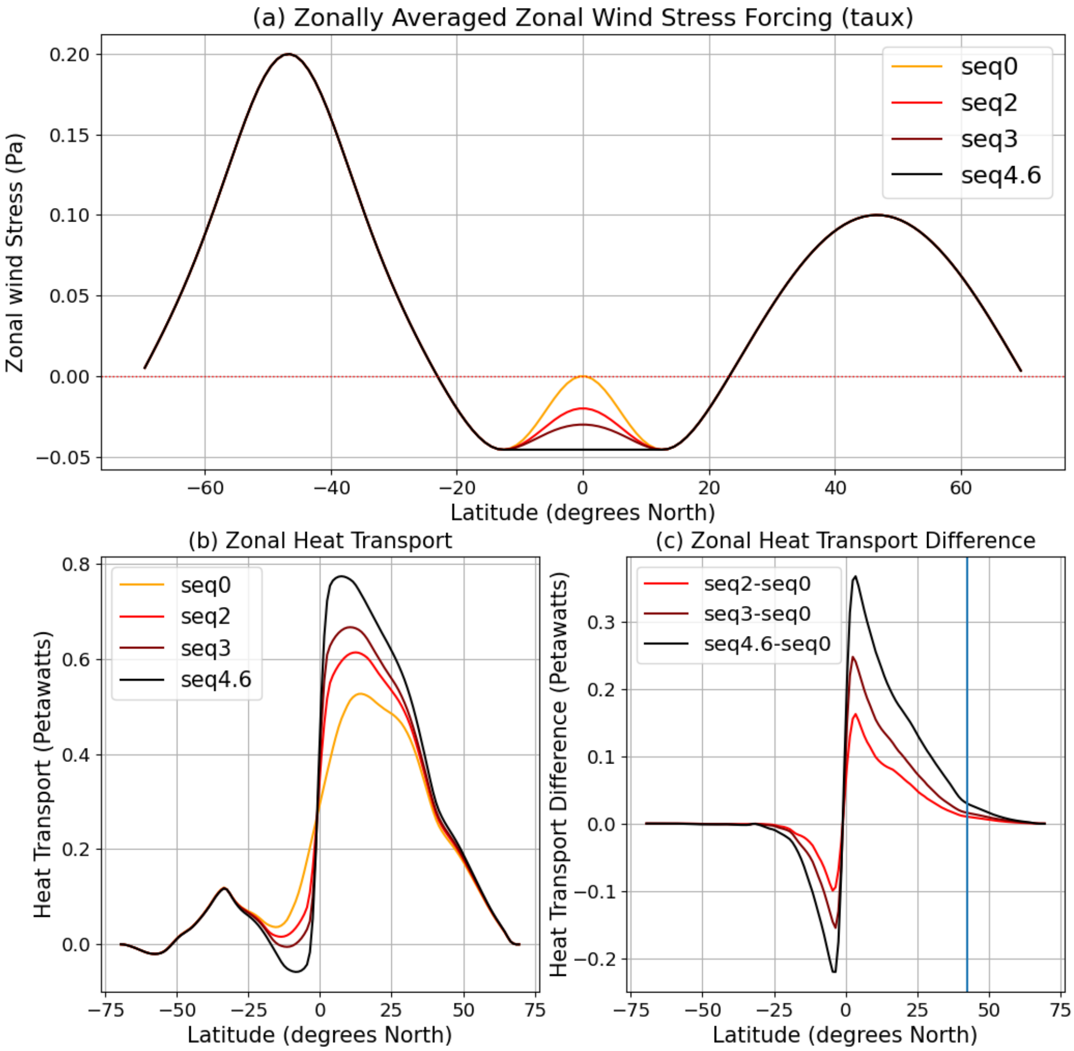

Fig. 2. (a) Latitude profile of zonally averaged wind stress forcings for 4 cases set as - 0 at the equator (orange), 0.02 westwards at the equator (red), 0.03 westwards at the equator (maroon), no curl between the tropical gyres in the North and South Hemispheres (black), set at 0.046 westwards between 12.5°S to 12.5°N. (b) Latitude profile of net heat transport by the AMOC in seq0, seq2, seq3, seq4.6. (c) Latitude profile of net heat transport of seq2, seq3 and seq4.6 differenced from seq0. The blue line is the poleward boundary of the Northern Hemisphere STG.

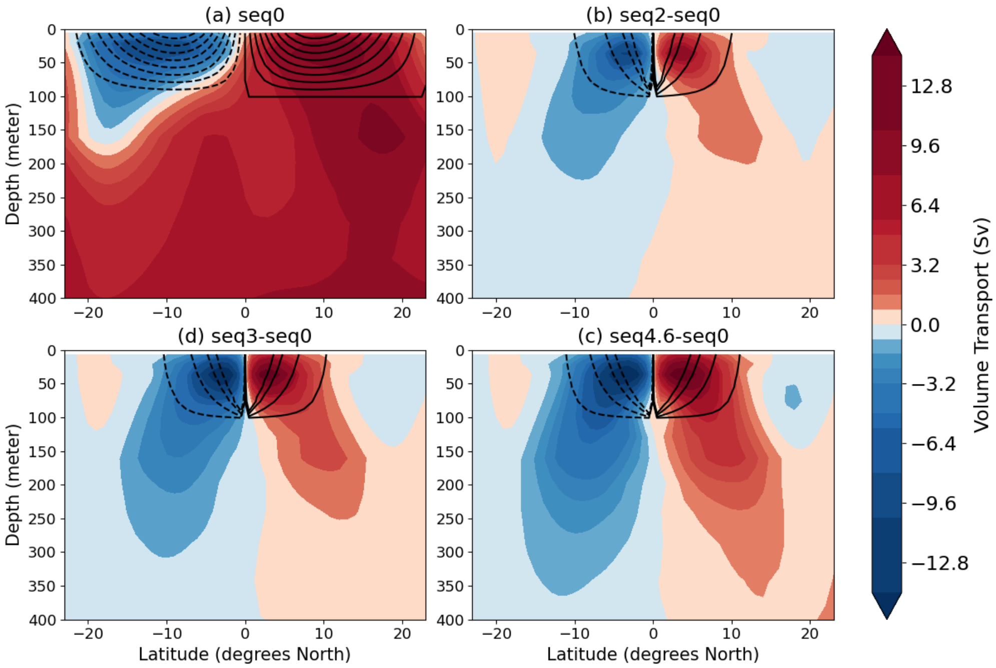

FIG. 3. a. Idealised volume transport contours from the Ekman transport of seq0 wind, overlapped on the ROC of the seq0 wind case as a function of latitude and depth ; b, c, d, Idealised volume transport contours from the Ekman transport of seq2, seq3, seq4.6 winds overlapped on ROC difference of seq2, seq3 and seq4.6 from seq0, respectively. Solid lines indicate a positive clockwise volumetric transport and dotted lines indicate a negative anticlockwise volumetric transport. The black contours have a spacing of 15 Sv in panels b, c, and d. We do not plot black contours higher than 40 Sv to avoid obscuring the shaded contours.

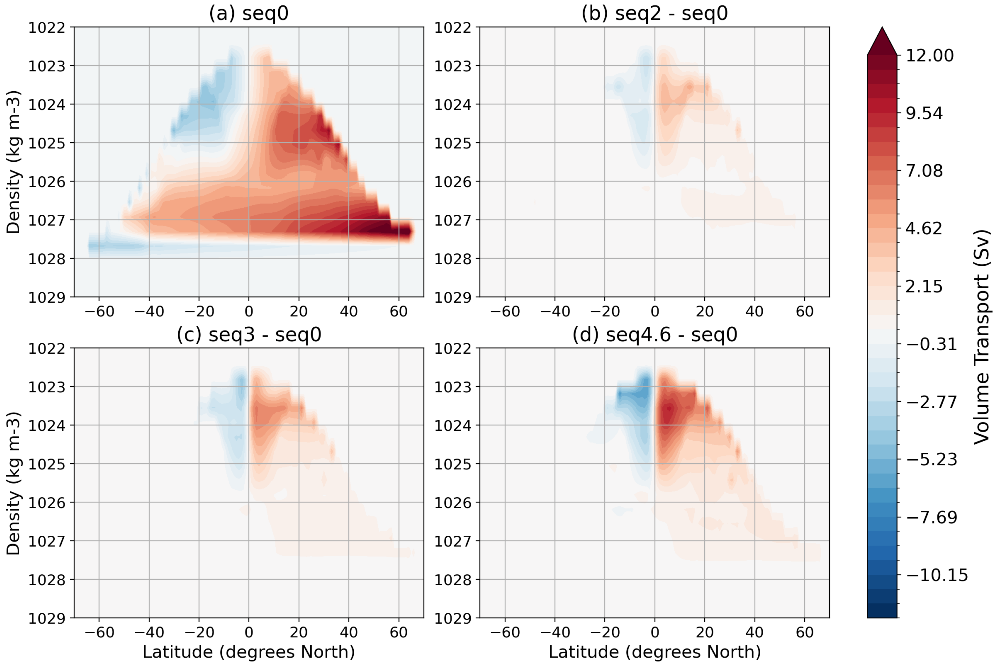

FIG. 4. a. Residual Overturning Circulation of the seq0 wind case as a function of latitude and density; b, c, d, Residual Overturning Circulation of seq0 subtracted from the ROC of seq2, seq3 and seq4.6 respectively. This shows the difference in the volumetric flow of water in reference to the seq0 run, for each of three the wind cases as a function of density.

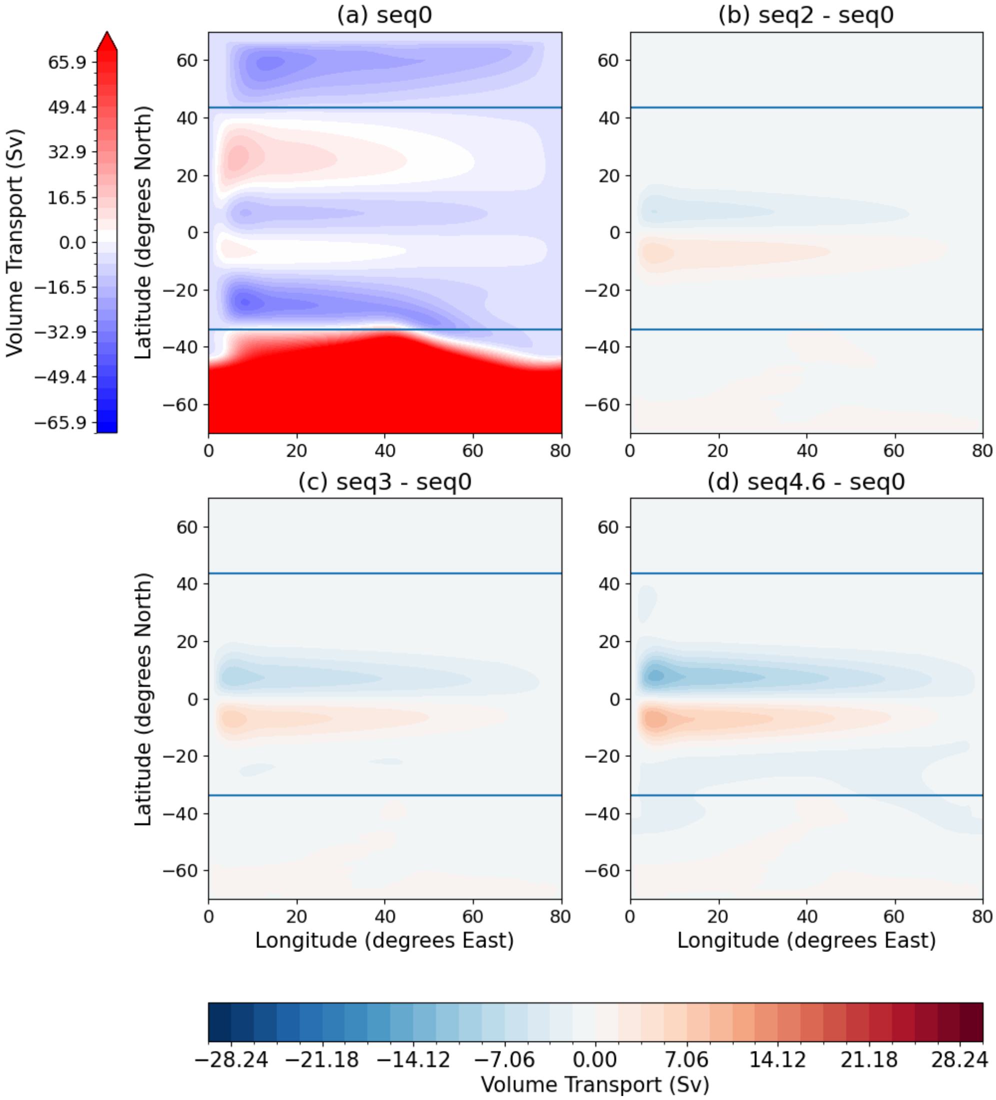

FIG. 5. a. Barotropic Streamfunction of the AMOC with seq0 forcing, with an indicative line at the poleward boundary of the STG latitudes. b,c,d barotropic streamfunction of seq0 subtracted from the barotropic streamfunction of seq2, seq3 and seq4.6 respectively, to show the change in the circulation on changing winds. Note the difference in the colorbars in two panels due a difference in the scaling in the volume transport, and a change in the volume transport. The blue lines indicate the edge of the subtropical gyres

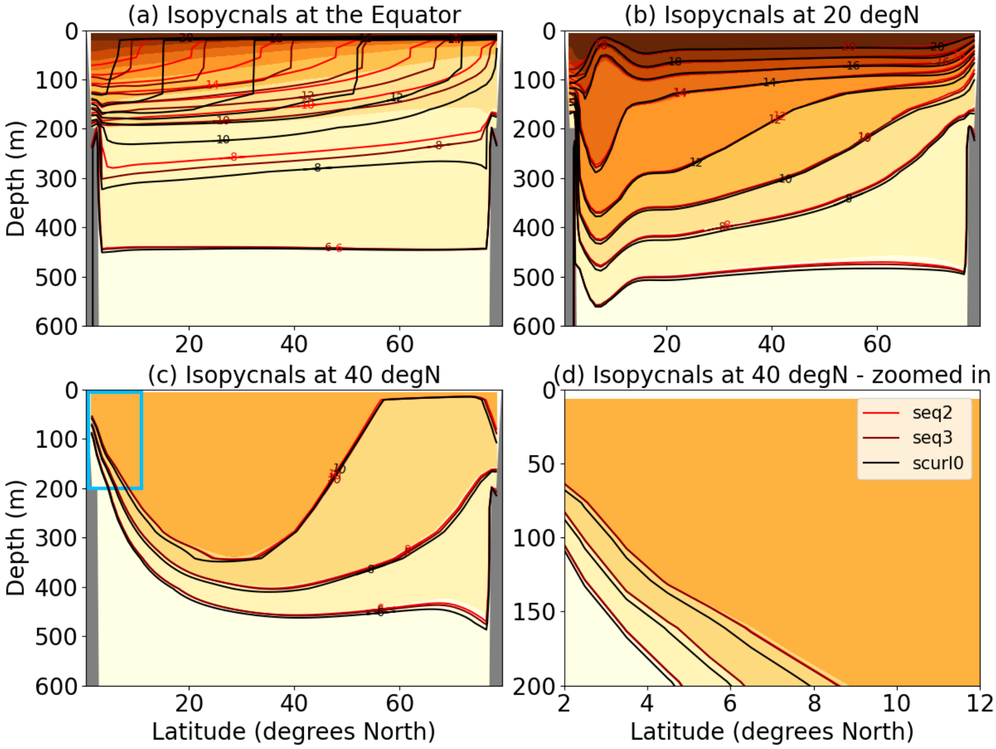

FIG. 6. Zonal cross section of the isopycnals of seq2 (red), seq3 (maroon), and seq4.6 (black) plotted on top of the zonal cross section of the isopycnal contours of seq0, for every 20 degree interval from the equator till 40°N. The contours of the 40°S are zoomed in on the Western Boundary (blue box). The isotherms are set at every 2° interval from 6°C to 20°C. The black boundaries indicate the walls of the channel

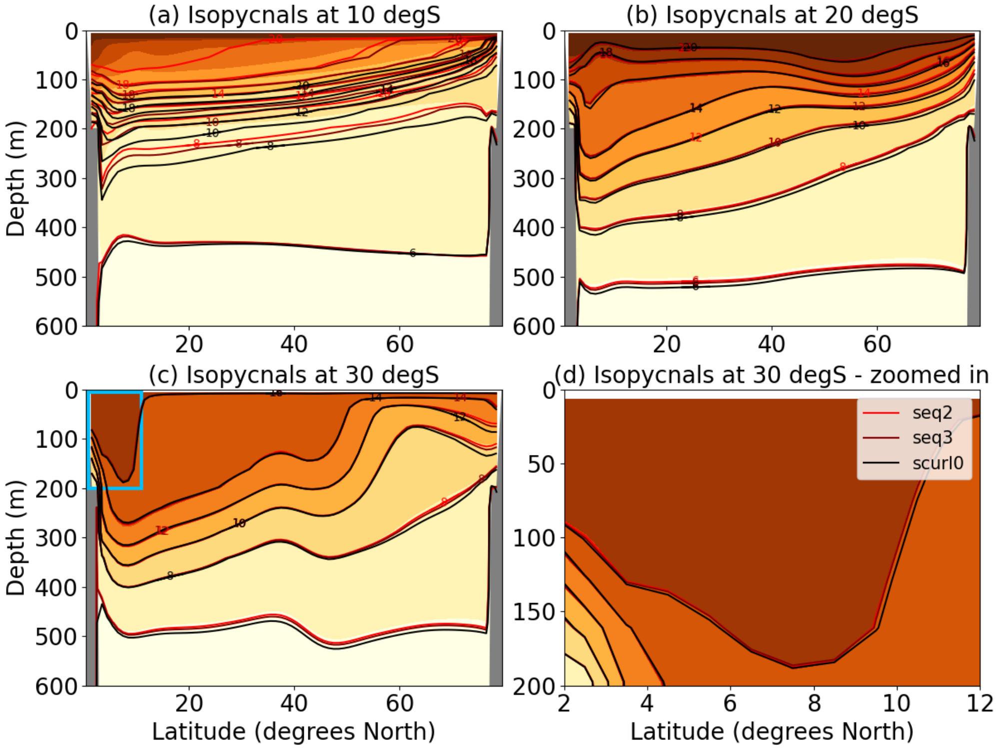

Fig. 7. Zonal cross section of the isopycnals of seq2 (red), seq3 (maroon), and seq4.6 (black) plotted on top of the zonal cross section of the isopycnal contours of seq0, for every 10 degree interval from the 10°S till 30°S. The contours of the 30°S are zoomed in on the Western Boundary (blue box). The isotherms are set at every 2° interval from 6°C to 20°C. The black boundaries indicate the walls of the channel

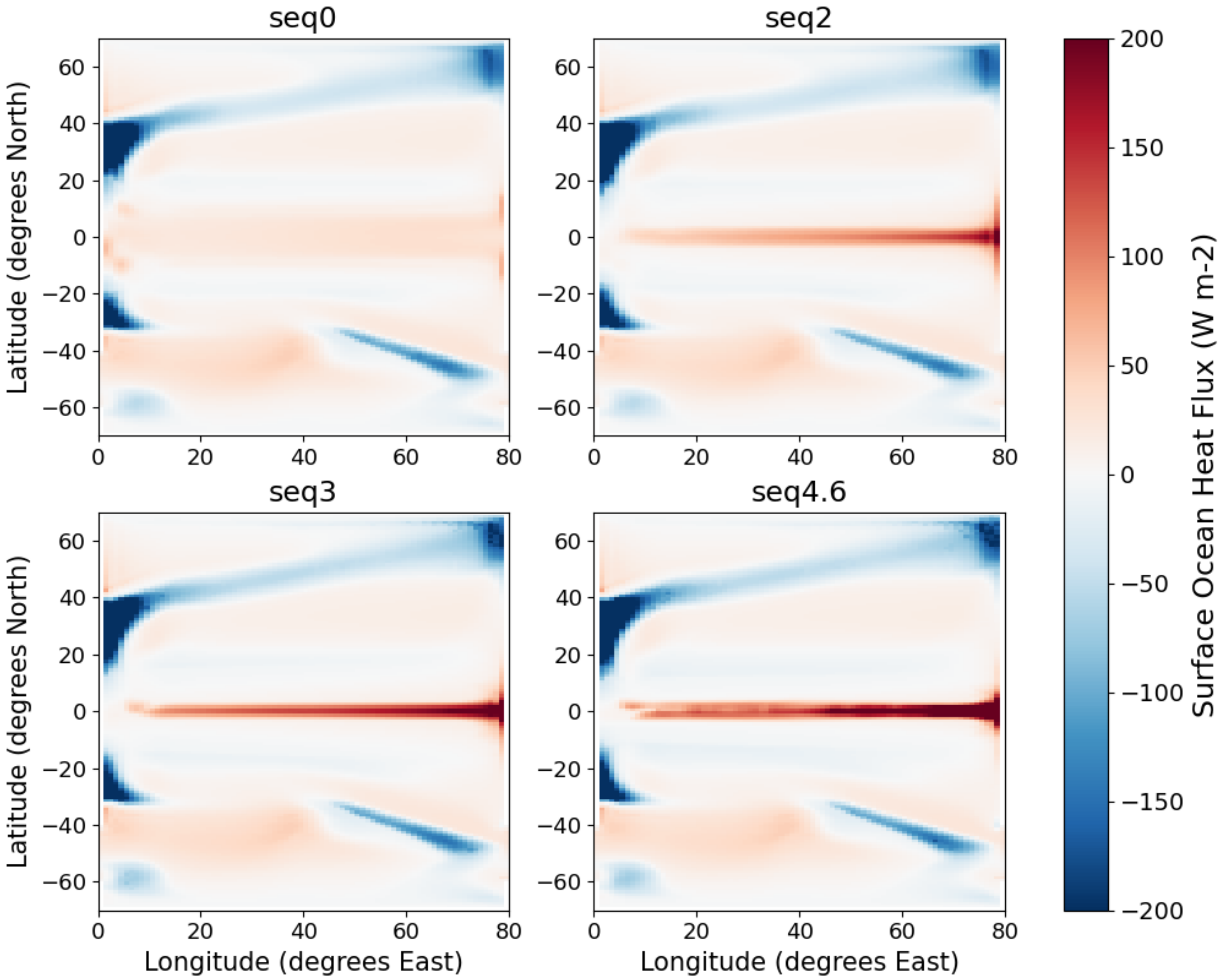

FIG. 8. Net Surface Heat Flux of the Ocean Basin for seq0, seq2, seq3, seq4.6. We see a high heat influx at the eastern boundary of the basin at the equator, consistent with our understanding of higher Ekman equatorial upwelling with higher winds

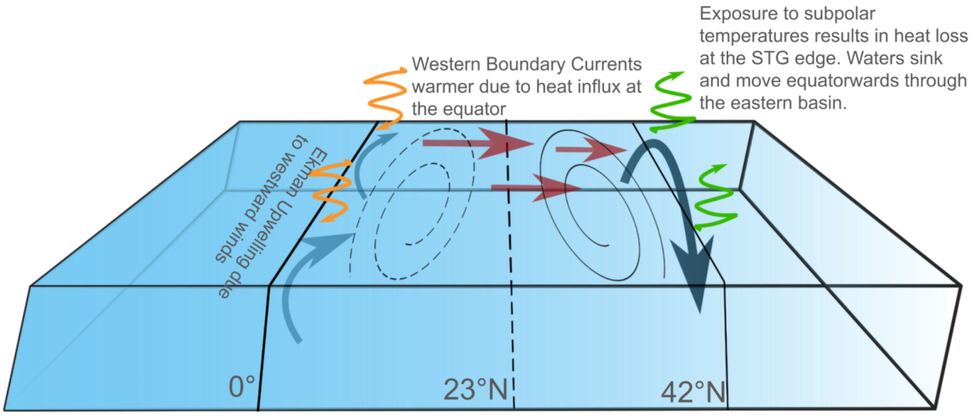

Fig. 9. Circulation pathway of water in the Northern Hemisphere, depicting the upwelling of water at the equator (which increases with increasing winds), and warmer waters traveling northwards through the western boundary currents. Upon reaching the STG, they downwell, and travel equatorwards through the eastern boundary, and eventually upwell at the equator, thus completing the circuit.

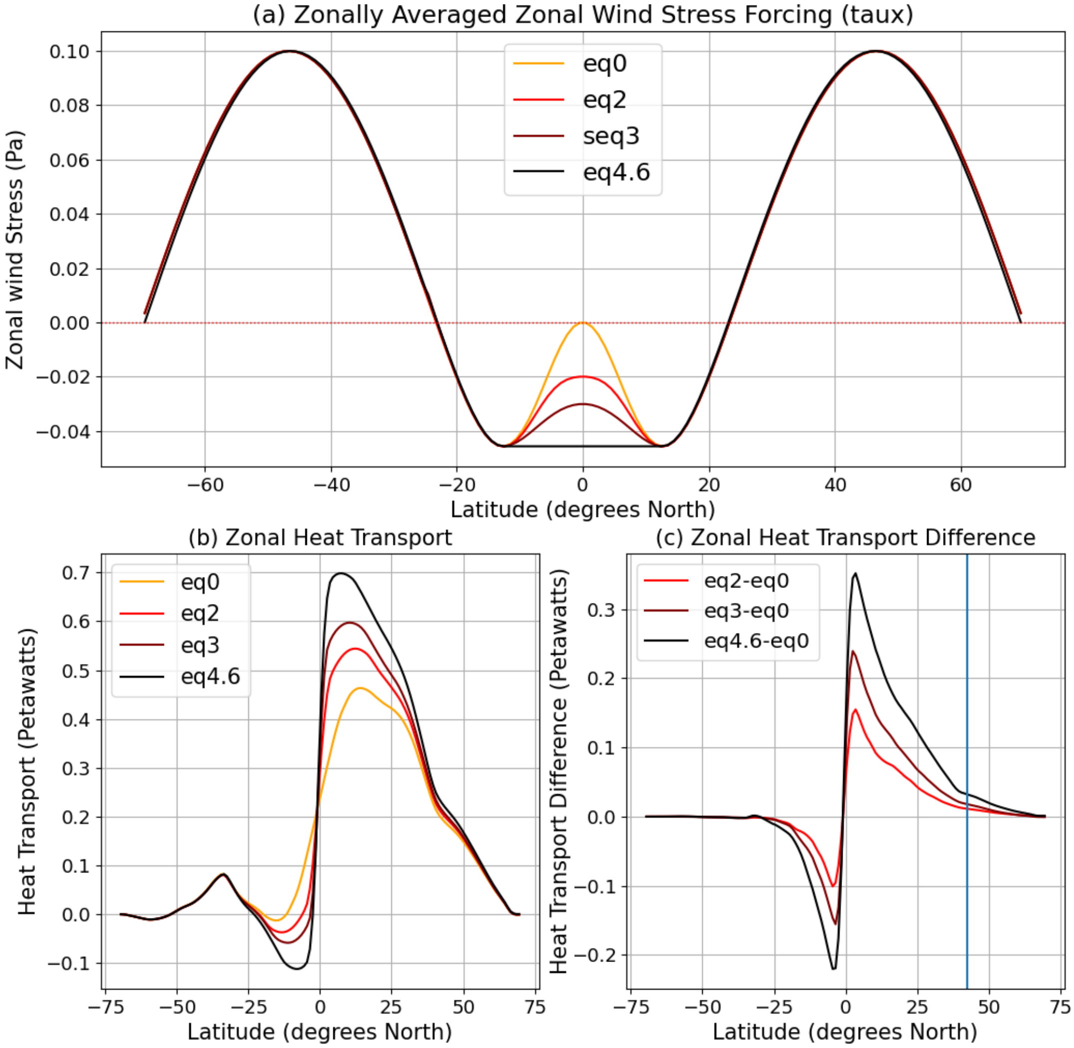

FIG. 10. (a) Latitude profile of zonally averaged wind stress forcings for 4 cases set as - 0 at the equator (orange), 0.02 westwards at the equator (red), 0.03 westwards at the equator (maroon), no curl between the tropical gyres in the North and South Hemispheres (black), set at 0.046 westwards between 12.5°S to 12.5°N. (b) Latitude profile of zonally averaged net heat transport by the AMOC in eq0, eq2, eq3, eq4.6. (c) Latitude profile of zonally averaged net heat transport of eq2, eq3 and eq4.6 differenced from seq0

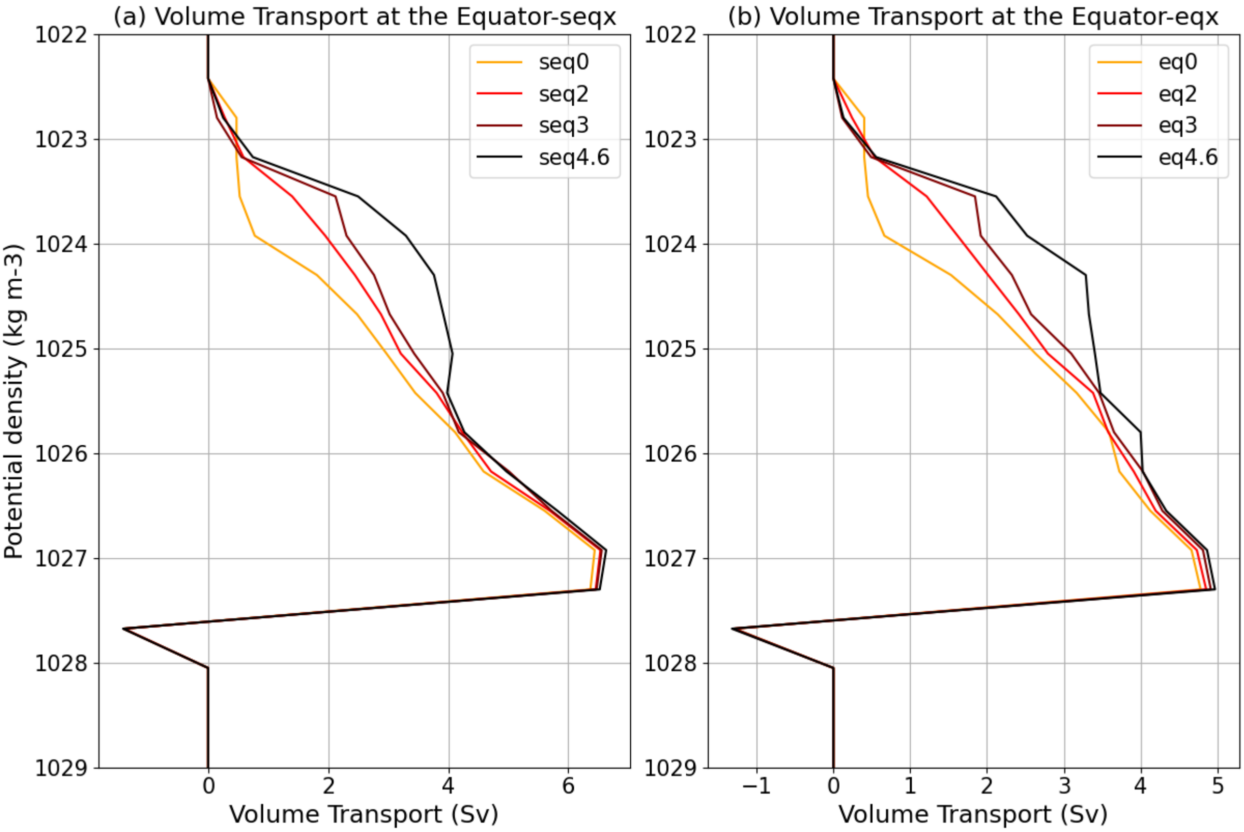

FIG. 11. Volume transport at the equator for the (a) seqx series and (b) eqx series

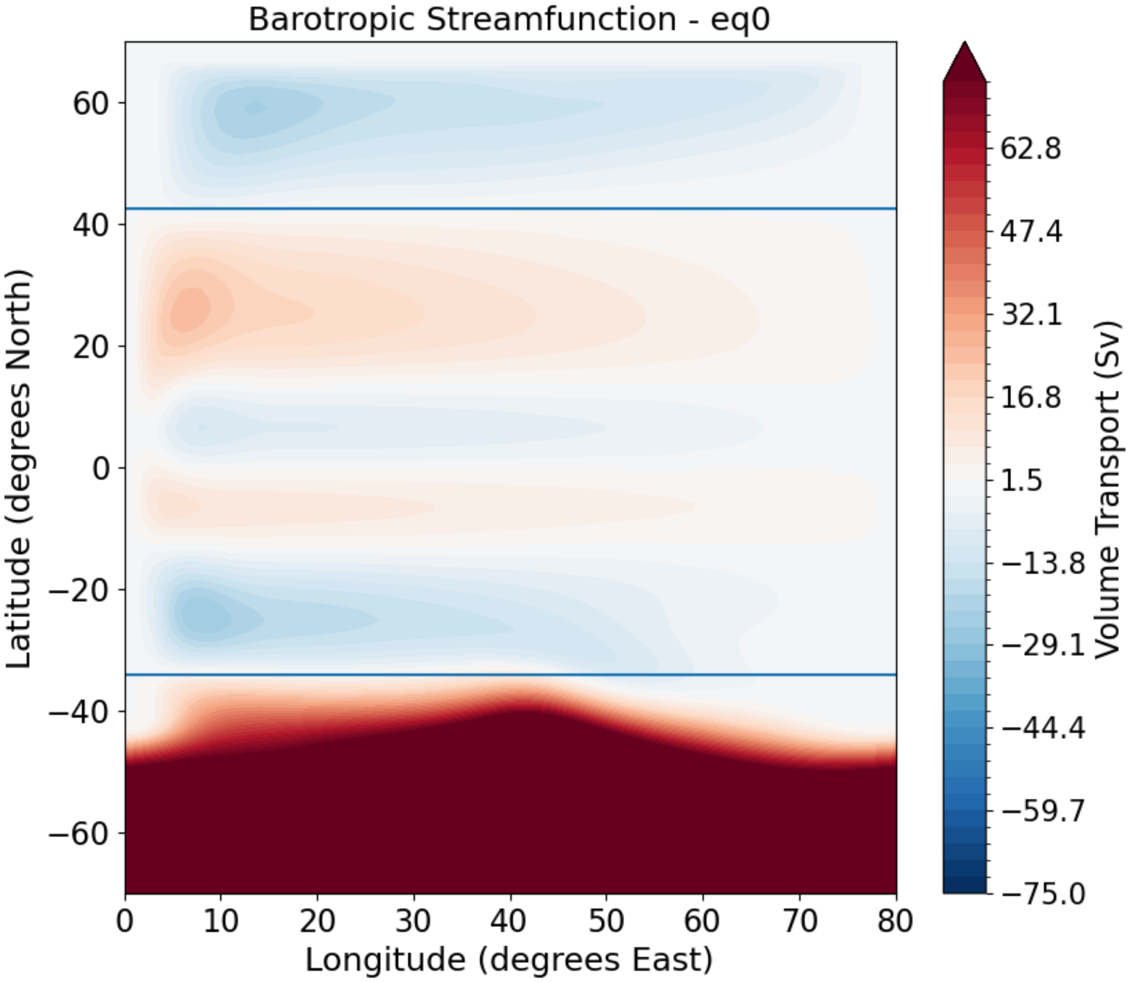

516 FIG. 12. Barotropic Streamfunction of the AMOC with eq0 forcing, with an indicative line at the poleward
517 boundary of the STG latitudes

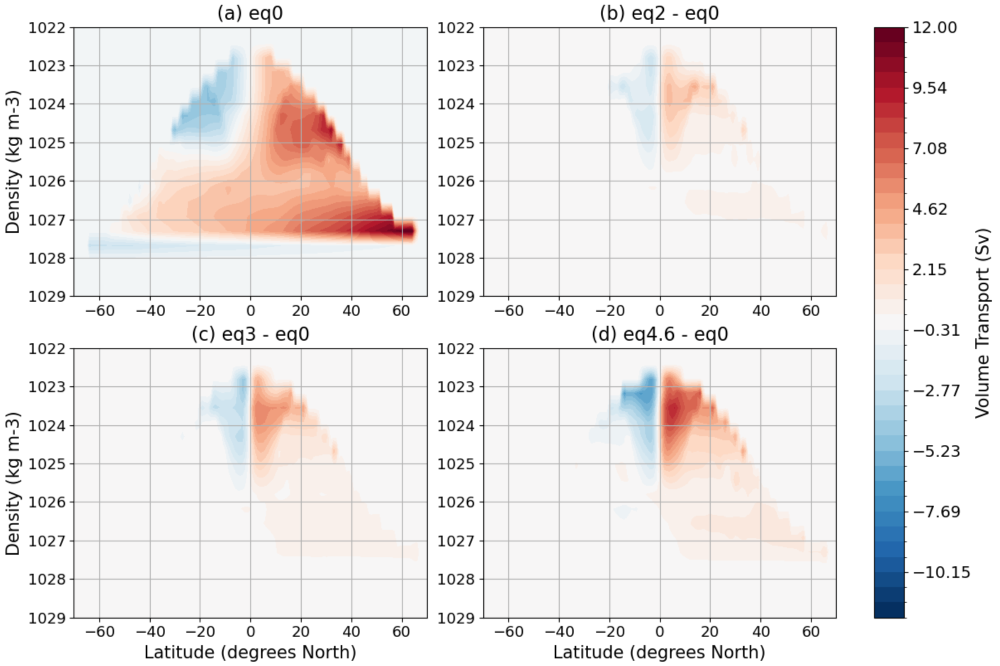

FIG. 13. a. Residual Overturning Circulation of the seq0 wind case as a function of latitude and density; b, c, d, Residual Overturning Circulation of eq0 subtracted from the ROC of eq2, eq3 and eq4.6 respectively. This shows the difference in the volumetric flow of water in reference to the eq0 run, for each of three the wind cases as a function of density.

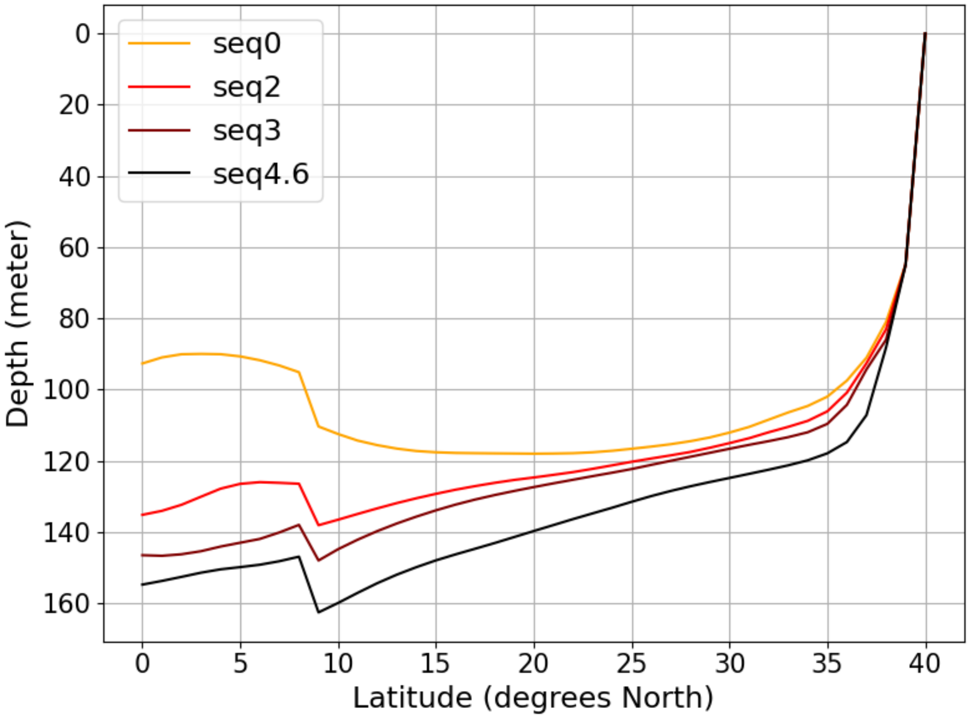

FIG. 14. Depth of the 10°C isotherm at the western boundary of the basin from the equator till 40°N

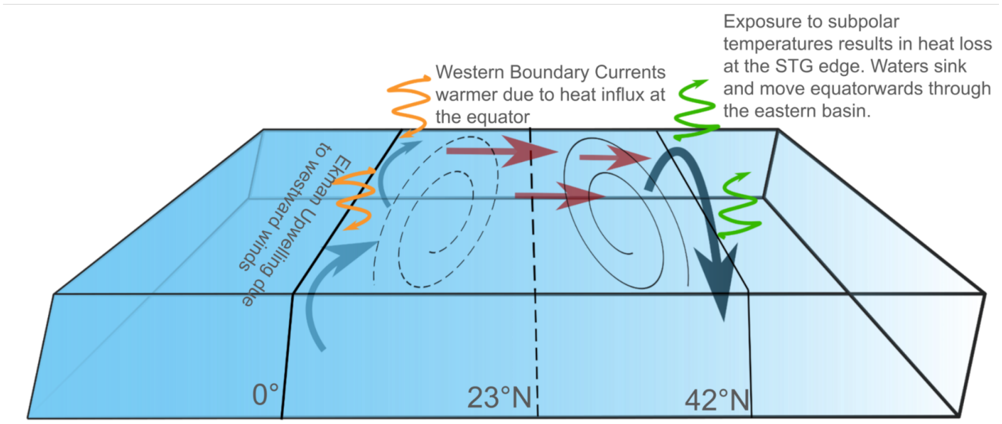

Fig. 15. Circulation pathway of water in the Northern Hemisphere, depicting the upwelling of water at the equator (which increases with increasing winds), and warmer waters traveling northwards through the western boundary currents. Upon reaching the STG, they downwell, and travel equatorwards through the eastern boundary, and eventually upwell at the equator, thus completing the circuit.

1. Supplementary Material

LIST OF FIGURES

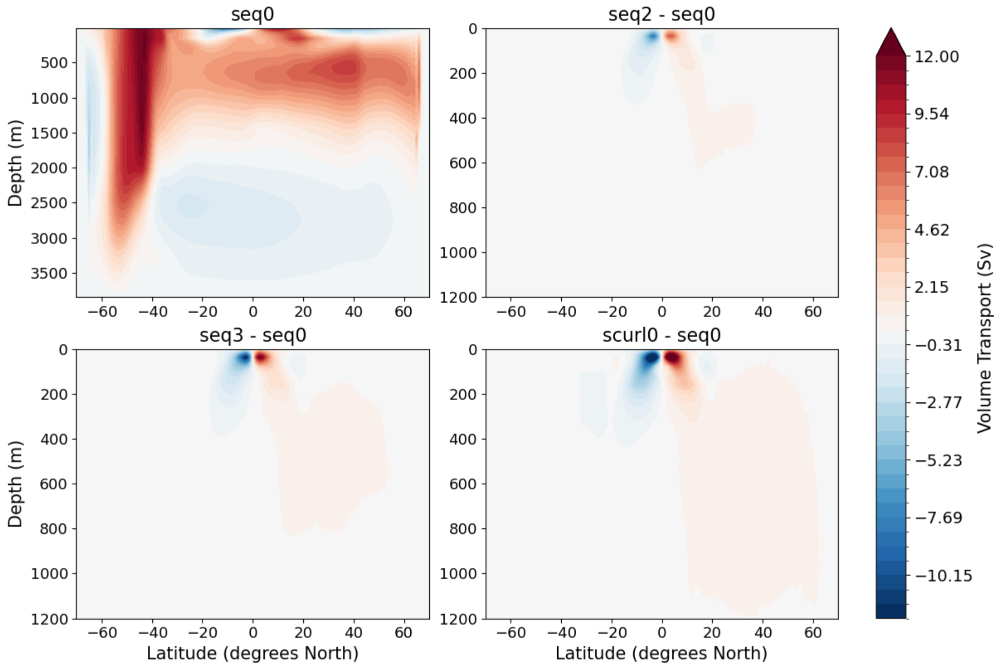

FIG. 1. a. ROC of the seq0 wind case as a function of latitude and depth ; b, c, d, ROC difference of seq2, seq3 and seq4.6 with seq0, respectively.

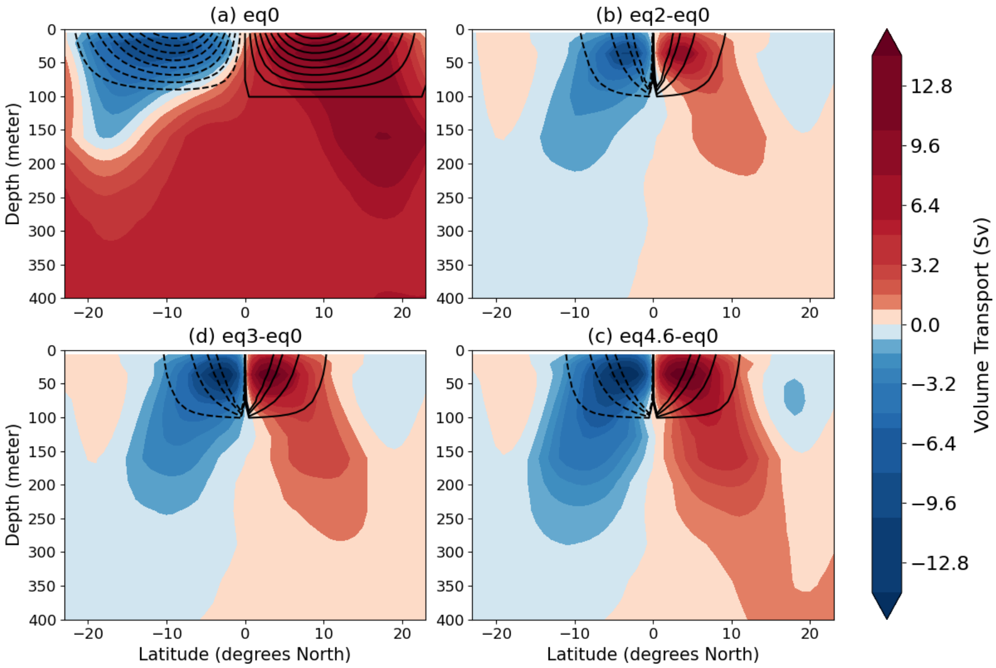

FIG. 2. a. Idealised volume transport contours from the Ekman transport of seq0 wind, overlapped on the ROC of the eq0 wind case as a function of latitude and depth ; b, c, d, Idealised volume transport contours from the Ekman transport of eq2, eq3, eq4.6 winds overlapped on ROC difference of eq2, eq3 and eq4.6 from seq0, respectively. Solid lines indicate a positive clockwise volumetric transport and dotted lines indicate a negative anticlockwise volumetric transport. The black contours have a spacing of 15 Sv in panels b, c, and d. We do not plot black contours higher than 40 Sv to avoid obscuring the shaded contours

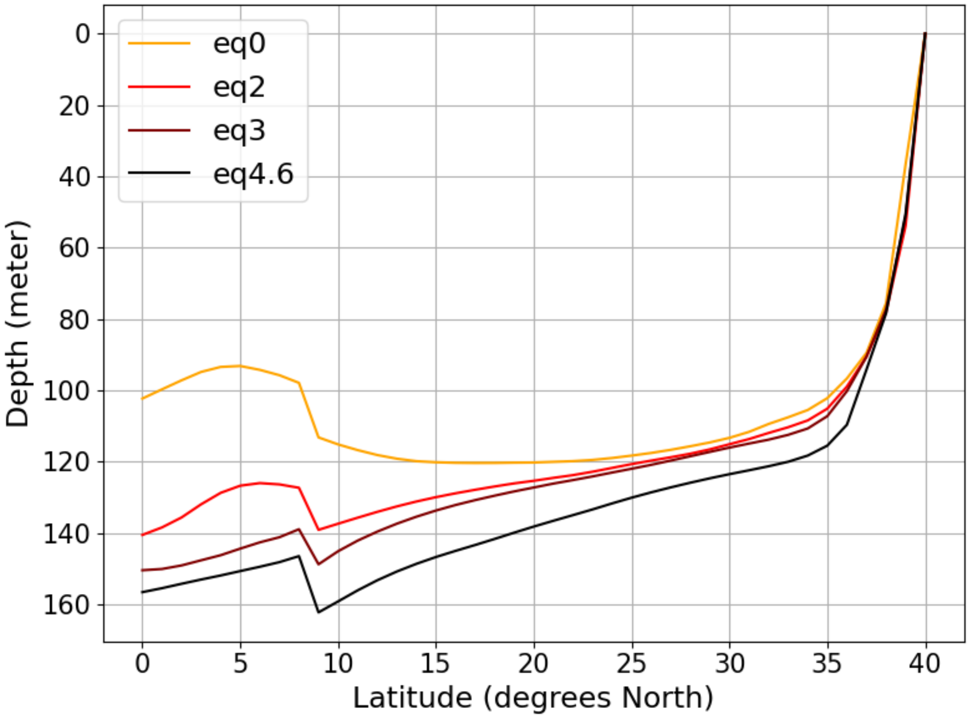

FIG. 3. Depth of the 10°C isotherm at the western boundary of the basin from the equator till 40°N for the eqx runs

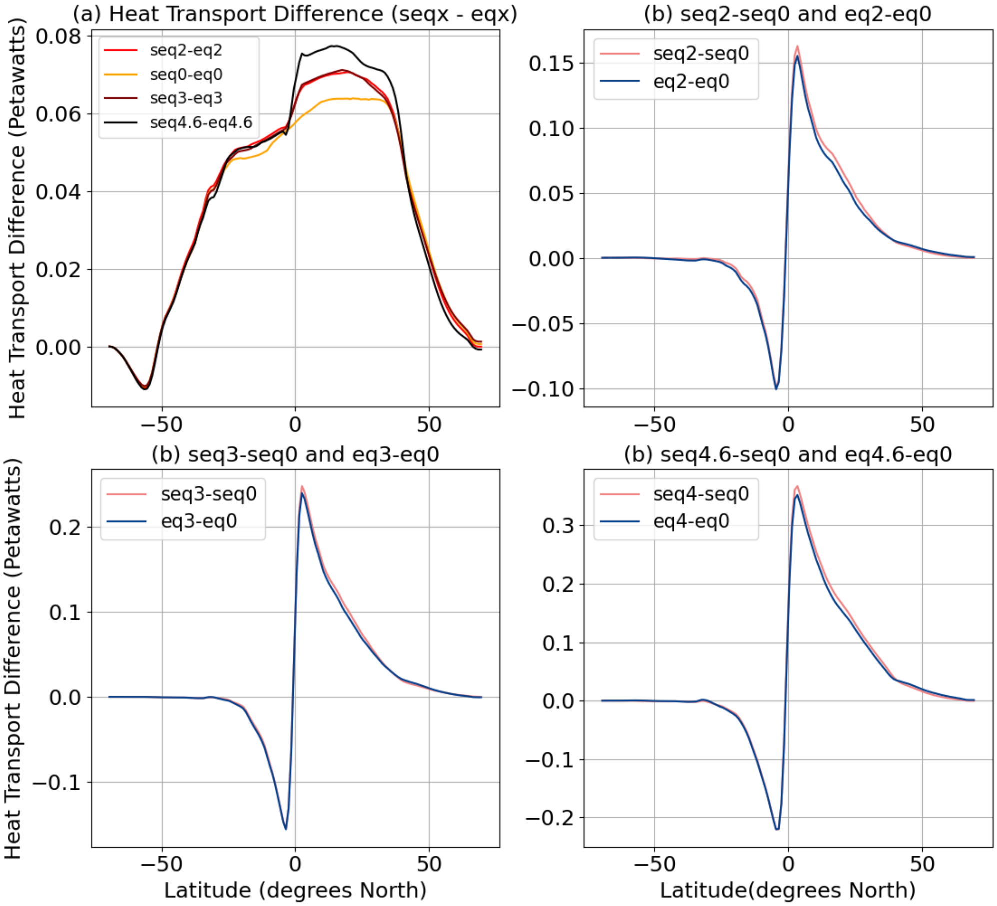

FIG. 4. (a) Difference of the heat transport in the eqx series subtracted from the heat transport in the seqx series. (b), (c) and (d) are the plots of the heat transport differences (with the control run) between the seqx and eqx experiments

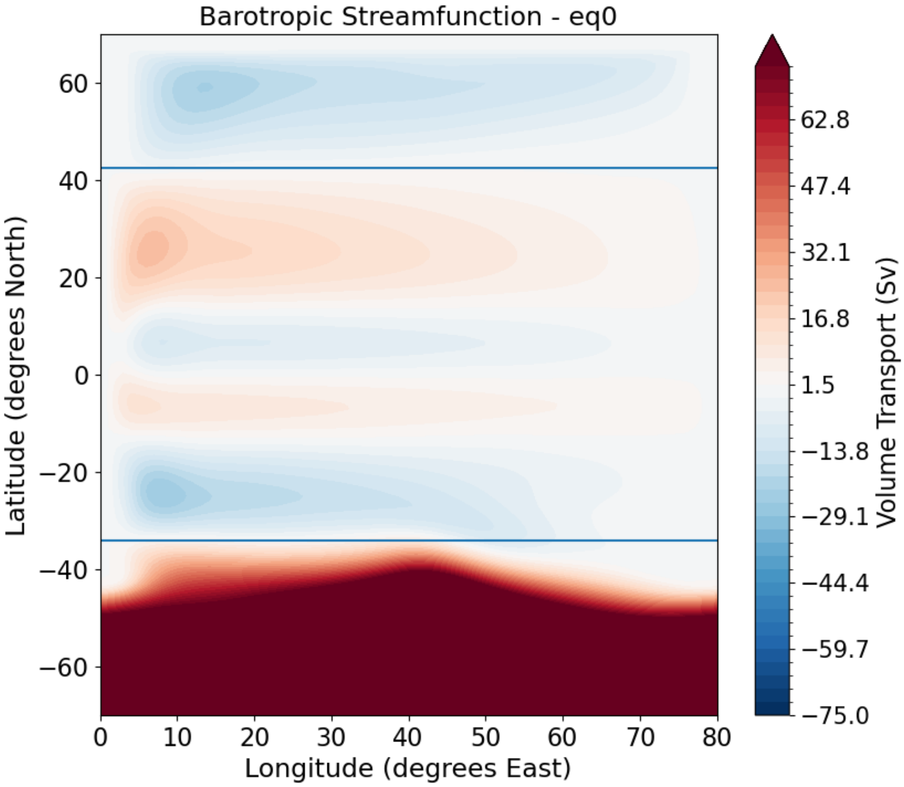

Fig. 5. Barotropic Streamfunction of the AMOC with eq0 forcing, with an indicative line at the poleward boundary of the STG latitudes